Formation of antiprotonic helium $\bar{p}He^+$ and ionization in low-energy collisions of $\bar{p}$ with He in the ground $1\,^1S$ and metastable $2\,^3S$ and $2\,^1S$ states

Kazuhiro Sakimoto

Institute of Space and Astronautical Science, Japan Aerospace Exploration Agency, Yoshinodai 3-1-1, Chuo-ku, Sagamihara 252-5210, Japan

(Received 17 February 2015; published 9 April 2015)

Calculations of low-energy collisions of antiprotons $\bar{p}$ with helium atoms in the ground ($1\,^1S$) and metastable ($2\,^3S$ and $2\,^1S$) states are carried out by using a semiclassical method and by further assuming that one of the two electrons is passive. Antiproton capture to form antiprotonic helium ($\rightarrow \bar{p}He^+ + e$) and breakup ionization ($\rightarrow \bar{p} + He^+ + e$) are investigated. The energy dependence of the capture and ionization cross sections and the distributions of the product states are presented and compared with previous theoretical calculations. For the metastable helium targets, most of the $\bar{p}He^+$ atoms produced in the capture have long lifetimes against subsequent Auger decays and can be observed experimentally. For the ground-state targets, however, the formation of such long-lived states is rather a rare event at low collision energies.

DOI: 10.1103/PhysRevA.91.042502 PACS number(s): 36.10.Gv, 34.50.Fa

I. INTRODUCTION

Antiprotonic helium $\bar{p}He^+$ is an exotic atom composed of an α particle (He^{2+}), an electron (e), and an antiproton ($\bar{p}$) which is a heavy negatively charged particle. The presence of $\bar{p}He^+$ was confirmed experimentally in $\bar{p}$ stopping in He [1,2], and since then high-resolution spectroscopic studies of $\bar{p}He^+$ have been vigorously carried on [3–5]. The $\bar{p}He^+$ atom is produced in capture of $\bar{p}$ by He, i.e., $\bar{p} + He \rightarrow \bar{p}He^+ + e$. In this reaction, the emitted electron can carry away only a small amount of kinetic energy owing to its lightness, and hence the antiproton is captured into an orbital having binding energy comparable with or smaller than that of the displaced electron: In other words, this $\bar{p}$ orbital possesses considerable internal energy measured from the atomic ground level of $\bar{p}He^+$ (~ -80 keV). For this reason, the $\bar{p}He^+$ atoms produced are intrinsically unstable due to Auger decay ($\rightarrow \bar{p}He^{2+} + e$), and cannot be observed in experiments unless they have sufficiently long lifetimes. As suggested by Condo [6] and Russell [7], a long lifetime can be achieved if the antiproton is captured into a circular or near-circular orbital. It seems that such an orbital is produced less frequently in the capture reaction. This accounts for the experimental fact that the total amount of $\bar{p}He^+$ detected in the measurements is a small but non-negligible fraction ($\sim$3%) of antiprotons stopped in He [1–3].

Other than near-circular states, the possibility of the existence of long-lived antiprotonic atoms has been suggested by several workers [8–12]: The Auger transition can be strongly suppressed whenever the angular momentum of the $\bar{p}$ orbital is sufficiently high. Such high-angular-momentum states can be produced in $\bar{p}$ capture by Li [10–12], where the $2s$ electron is involved. Although the same situation is expected to occur for the He target in excited metastable $2S$ states [9,12], no further investigation appears to have been made yet of $\bar{p}$ capture by metastable He.

So far, there are several theoretical calculations for $\bar{p}$ capture by He in the ground ($1\,^1S$) state: e.g., the diabatic-state treatment [13], the coupled-channel semiclassical approximation [14], the adiabatic hidden-crossing theory [15], the Born approximation [16], the classical trajectory Monte Carlo method [17], and the fermion molecular dynamics (FMD) method [18,19]. Only in the FMD method are two electrons allowed to participate in the dynamical process. Earlier major calculations of $\bar{p}$ + He are summarized in Ref. [20]. Although rigorous full quantum-mechanical (QM) calculations have been carried out for the $\bar{p}$ + H system [21–24], such a treatment of the four-body system of $\bar{p}$ + He is far beyond the present computer capacity. Only recently was a QM calculation applied to $\bar{p}$ + He by assuming it to be an effective one-electron system [25].

The present paper investigates in detail $\bar{p}$ capture by He in the ground ($1\,^1S$) and metastable ($2\,^3S$ and $2\,^1S$) states by using a semiclassical (SC) method [12,26], in which the radial distance between $\bar{p}$ and He^{2+} is treated as a classical variable, and the other degrees of freedom are fully described by quantum mechanics. In contrast to the QM calculation [25], which is limited to the capture process at low collision energies, also considered here is breakup ionization, $\bar{p} + He \rightarrow \bar{p} + He^+ + e$, which becomes open at energies above the first ionization threshold. The SC method has been applied to the $\bar{p}$ + H [26] and $\bar{p}$ + Li [12] systems, but apparently not yet to the $\bar{p}$ + He system. For $\bar{p}$ + H, agreement between the SC and QM results for the reactive cross sections is good at collision energies both below and above the ionization threshold [22,26]. In Ref. [12], the adequacy of the SC method for calculating the distribution of the product states was further established by making a comparison between the SC and QM results for negative muon (μ^-) capture by H. Thus, the SC method is expected to be sufficiently useful for the present purpose. Unfortunately, an accurate treatment of two electrons is still quite difficult even within the SC approximation. In the present study, only one electron is assumed to play a dynamical role in the reaction process. This effective one-electron model is the same as that introduced in most of the previous studies [13–15,17,25].

The present paper is arranged as follows: In Sec. II, the SC treatment based on the one-electron approximation is summarized. In Sec. III, the stability of $\bar{p}He^+$ against Auger decay is briefly discussed by using the Born-Oppenheimer (BO) potential energy curves. The results of the state distributions and the cross sections in the capture and ionization processes are presented for the ground $1\,^1S$ state of the He target in

Sec. IV and for the metastable $2\,^3S$ and $2\,^1S$ states in Sec. V. Then the possibility of producing long-lived $\bar{p}\mathrm{He}^+$ in $\bar{p}+\mathrm{He}$ collisions is examined. Finally, Sec. VI summarizes the present results, and gives some consideration to previous studies dealing with the ionization of He by high-energy (>1 keV) $\bar{p}$ impacts.

II. THEORY

A. Interaction

In the present study, the effective one-electron model is introduced, and the interaction V of the $\bar{p}+\mathrm{He}$ system is given by the sum of two-body terms, i.e.,

$$V = V_{e\text{-He}^+}(r) + \frac{1}{|\mathbf{R}-\mathbf{r}|} + V_{\bar{p}\text{-He}^+}(R), \tag{1}$$

where $\mathbf{r}$ is the position vector of e from He^+, and $\mathbf{R}$ is that of $\bar{p}$ from He^+. Here and in the following, atomic units are used unless otherwise stated. This interaction form was employed also in the QM study of Tong *et al.* [25]. For the electron interaction $V_{e\text{-He}^+}(r)$ with the He^+ core, adopted here is a spin-dependent model potential constructed by Rabli *et al.* [27], who investigated electronic excitation and charge transfer in $\mathrm{He}^{2+}+\mathrm{He}$ collisions. In the present calculation, the He target states of $1s^2\,(1\,^1S)$, $1s2s\,(2\,^3S)$, and $1s2s\,(2\,^1S)$ are considered, and the use of this model potential offers the first ionization potentials of He, $I_{1\,^1S}=0.8989$ a.u., $I_{2\,^3S}=0.1749$ a.u., and $I_{2\,^1S}=0.1462$ a.u. [27], which agree reasonably well with experimental values [28]. The interaction $V_{\bar{p}\text{-He}^+}(R)$ between $\bar{p}$ and He^+ may be obtained by assuming the BO approximation. The BO potential of $\bar{p}+\mathrm{He}^+$ was investigated in detail and tabulated by Shimamura [29].

In $\bar{p}+\mathrm{H}$ collisions, the relative motion is found to be governed by the BO potential [26]. In the present study, the BO potential is again assumed to be suitable for describing the $\bar{p}+\mathrm{He}$ motion. For the active electron in the $\bar{p}+\mathrm{He}$ system, the adiabatic wave function $\chi_\gamma(\mathbf{r};R)$ is calculated by solving [12,27]

$$\tilde{H}_0\frac{1}{r}\chi_\gamma(\mathbf{r};R) = \mathcal{E}_\gamma(R)\frac{1}{r}\chi_\gamma(\mathbf{r};R), \tag{2}$$

where

$$\tilde{H}_0 = -\frac{1}{2r}\frac{\partial^2}{\partial r^2}r + \frac{\tilde{\mathbf{l}}^2}{2r^2} + V_{e\text{-He}^+}(r) + \frac{1}{|\mathbf{R}-\mathbf{r}|}, \tag{3}$$

with $\tilde{\mathbf{l}}$ being the electron angular momentum operator. Equation (2) depends parametrically on R, and the index γ indicates the He state (i.e., $\gamma = 1\,^1S$, $2\,^3S$, and $2\,^1S$) in the separated-atom limit ($R\to\infty$). In the present model, the BO potential of the total system $\bar{p}+\mathrm{He}$ may be given by

$$U(R) = \mathcal{E}_\gamma(R) + I_\gamma + V_{\bar{p}\text{-He}^+}(R). \tag{4}$$

When R is large, the electron energy $\mathcal{E}_\gamma(R)$ can be expressed as $-I_\gamma + 1/R - C_\gamma/R^4$ with a constant C_γ, and the interaction $V_{\bar{p}\text{-He}^+}(R)$ becomes $-1/R - C_\gamma^+/R^4$ with a constant C_γ^+ [29]. Therefore, the BO potential has the asymptotic form

$$U(R) \to -\frac{\alpha_\gamma}{2R^4}, \tag{5}$$

where $\alpha_\gamma = 2(C_\gamma + C_\gamma^+)$ can be regarded as the polarizability of $\mathrm{He}(\gamma)$. By assuming this asymptotic form at a large value of R, one can calculate the polarizability α_γ: The present calculation yields $\alpha_{1\,^1S}=0.949$ a.u., $\alpha_{2\,^3S}=374.6$ a.u., and $\alpha_{2\,^1S}=807.4$ a.u., while the values of previous detailed calculations [30,31] are $\alpha_{1\,^1S}=1.383$ a.u., $\alpha_{2\,^3S}=315.92$ a.u., and $\alpha_{2\,^1S}=803.25$ a.u. The precision of the polarizability is not so good for the $1\,^1S$ state. The present calculation might underestimate the magnitude of the cross section for $\bar{p}$ capture by $\mathrm{He}(1\,^1S)$ if very low-energy ($\ll$1 eV) collisions were considered. The BO potential curves of $\bar{p}+\mathrm{He}^+$ and $\bar{p}+\mathrm{He}$ ($\gamma = 1\,^1S$ and $2\,^3S$) are plotted in the range of $R\leqslant 10$ a.u. in Fig. 1.

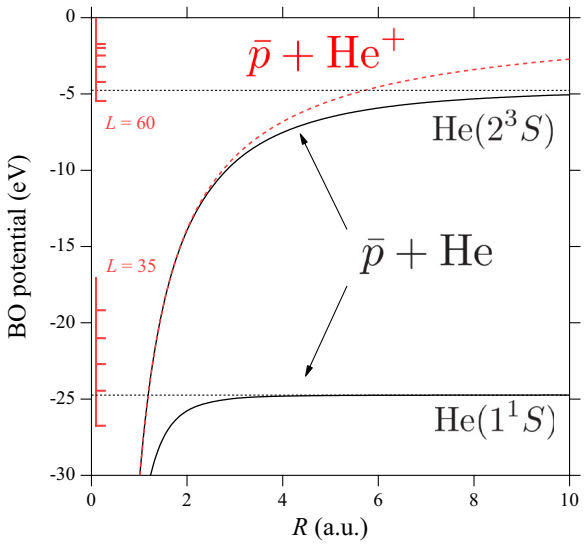

FIG. 1. (Color online) BO potential energies $U(R)-I_\gamma$ of $\bar{p}+\mathrm{He}$ ($\gamma = 1\,^1S$ and $2\,^3S$) and $V_{\bar{p}\text{-He}^+}(R)$ of $\bar{p}+\mathrm{He}^+$. Horizontal bars indicate several energy levels of $\bar{p}\mathrm{He}^+$ for the angular momenta $L=35$ and 60.

B. Collision calculation

In the present study, the radial distance R is assumed to be a classical variable, and the other dynamical variables $(\hat{\mathbf{R}},\mathbf{r})$ are described by quantum mechanics [12,26]. The quantum-mechanical part of the Hamiltonian is given by

$$\tilde{H} = \frac{\tilde{\mathbf{L}}^2}{2m_R R^2} + \tilde{H}_0, \tag{6}$$

where $\tilde{\mathbf{L}}$ is the angular momentum operator of $\bar{p}\mathrm{He}^+$, and m_R is the reduced mass of $\bar{p}+\mathrm{He}^+$. In the conventional SC method, the variables R and $\hat{\mathbf{R}}$ are treated together as classical. It should be mentioned that the numerical labor of the present SC method is almost the same as for the conventional one. Nevertheless, the conservation of the total angular momentum $\tilde{\mathbf{J}} = \tilde{\mathbf{L}} + \tilde{\mathbf{l}}$ is accurately taken into account in Eq. (6). This is a great advantage in discussing the angular momentum distribution of the capture products.

In the SC method, the time-dependent Schrödinger equation for $\bar{p}$ + He collisions becomes

$$i\frac{\partial}{\partial t}\Psi^{JM}(\hat{\mathbf{R}},\mathbf{r},t) = \tilde{H}\Psi^{JM}(\hat{\mathbf{R}},\mathbf{r},t). \tag{7}$$

The total wave function $\Psi^{JM}(\hat{\mathbf{R}},\mathbf{r},t)$ can be written in the form [26]

$$\Psi^{JM}(\hat{\mathbf{R}},\mathbf{r},t) = \frac{1}{r}\sum_{\lambda\geqslant 0}\mathcal{D}^{J}_{M\lambda}(\hat{\mathbf{R}})\psi^{J\lambda}(\mathbf{r},t) \times \exp\left[-i\int^{t}\frac{J(J+1)}{2m_R R^2}dt'\right], \tag{8}$$

where (J,M) are the total angular momentum quantum numbers,

$$\mathcal{D}^{J}_{M\lambda}(\hat{\mathbf{R}}) = \left[\frac{2J+1}{8\pi(1+\delta_{\lambda 0})}\right]^{1/2}\left[D^{J}_{M\lambda}(\hat{\mathbf{R}}) + (-1)^{\lambda}D^{J}_{M-\lambda}(\hat{\mathbf{R}})\right]^{*} \tag{9}$$

is the symmetrized and normalized form of the Wigner rotation matrix element $D^{J}_{M\lambda}(\hat{\mathbf{R}})$, and $\psi^{J\lambda}(\mathbf{r},t)$ is solved numerically. The actual details of the numerical calculation are exactly the same as in Ref. [12], and are not shown here.

The initial condition of $\Psi^{JM}(\hat{\mathbf{R}},\mathbf{r},t)$ is given by choosing

$$\psi^{J\lambda}(\mathbf{r},t=0) = \chi_{\gamma}(\mathbf{r};R_0)\,\delta_{\lambda 0}, \tag{10}$$

where $R_0 = R(t=0)$ is the initial radial distance. For the purpose of determining the time dependence $R(t)$, the following classical equation of motion is solved:

$$E = \frac{m_R}{2}\left(\frac{dR}{dt}\right)^2 + U_{\mathrm{eff}}(R), \tag{11}$$

where E is the collision energy of $\bar{p}$ + He, and

$$U_{\mathrm{eff}}(R) = \frac{(J+1/2)^2}{2m_R R^2} + U(R) \tag{12}$$

is the effective potential.

The probability density of the emitted electron having the kinetic energy ε is given by [12]

$$\frac{dP^{J}_{Ll}}{d\varepsilon} = \frac{1}{m_r}\mathrm{Im}\left[\left(A^{J}_{Ll}\right)^{*}\frac{dA^{J}_{Ll}}{dr}\right]_{r=r_0}, \tag{13}$$

where r_0 is taken to be sufficiently large, and

$$A^{J}_{Ll}(r,\varepsilon) = \frac{1}{\sqrt{2\pi}}\int \mathrm{e}^{i\varepsilon t}f^{J}_{Ll}(r,t)dt. \tag{14}$$

The function $f^{J}_{Ll}(r,t)$ in the integral is the wave packet of the emitted electron and can be calculated from $\psi^{J\lambda}(\mathbf{r},t)$ [12]: i.e.,

$$f^{J}_{Ll}(r,t) = \sum_{\lambda\geqslant 0}X^{Jl}_{L\lambda}\langle Y_{l\lambda}|\psi^{J\lambda}(t)\rangle_r, \tag{15}$$

where $Y_{l\lambda}(\hat{\mathbf{r}})$ is the spherical harmonics, and

$$X^{Jl}_{L\lambda} = \left(\frac{2L+1}{2J+1}\right)^{1/2}(L0l\lambda|J\lambda)\frac{1+(-1)^{J+L+l}}{[2(1+\delta_{\lambda 0})]^{1/2}}, \tag{16}$$

with the Clebsch-Gordan coefficient $(L0l\lambda|J\lambda)$.

C. Capture state analysis

First, let us consider the collision energies below the ionization threshold of He (i.e., $E < I_{\gamma}$). Then the event of e emission is identical to the event of $\bar{p}$ capture ($\rightarrow \bar{p}\mathrm{He}^+ + e$). In this case, the integration of $dP^{J}_{Ll}/d\varepsilon$ over ε and the summation over l yield the probability of the capture into the L state,

$$P^{J}_{L} = \sum_{l}\int\frac{dP^{J}_{Ll}}{d\varepsilon}d\varepsilon. \tag{17}$$

A further summation over L gives the total capture probability

$$P^{J}_{\mathrm{cap}} = \sum_{L}P^{J}_{L}. \tag{18}$$

The total capture cross section becomes

$$\sigma_{\mathrm{cap}} = \frac{\pi}{2m_R E}\Omega_{\mathrm{cap}}, \tag{19}$$

where

$$\Omega_{\mathrm{cap}} = \sum_{J}\Omega^{J}_{\mathrm{cap}}, \tag{20}$$

with

$$\Omega^{J}_{\mathrm{cap}} = (2J+1)P^{J}_{\mathrm{cap}}. \tag{21}$$

In order to determine the relation between the electron energy ε and the internal state of the $\bar{p}\mathrm{He}^+$ atom, the conservation rule of the total energy E_{tot} is employed [12,32]: i.e.,

$$E_{\mathrm{tot}} = E - I_{\gamma} = E_{NL} + \varepsilon, \tag{22}$$

where E_{NL} is the energy of the vibrational motion supported by the potential $V_{\bar{p}\text{-}\mathrm{He}^+}(R)$. The principal quantum number N of the $\bar{p}$ orbital in $\bar{p}\mathrm{He}^+$ can be defined by $N = v + L + 1$, where the vibrational quantum number v is calculated from its classical counterpart (i.e., action integral):

$$v + \frac{1}{2} = \frac{\sqrt{2m_R}}{\pi}\int_{R_1}^{R_2}\left[E_{NL} - \frac{(L+1/2)^2}{2m_R R^2} - V_{\bar{p}\text{-}\mathrm{He}^+}(R)\right]^{1/2}dR, \tag{23}$$

with R_1 and R_2 being the turning points of the vibrational motion. Figure 2 shows the quantum number N as a function of E_{NL} for the bound system of $\bar{p}\mathrm{He}^+$. It turns out that the energy level E_{NL} deviates greatly from the hydrogenic formula $-m_R/(2N^2)$ for $N < 100$. When one calculates the distribution of the $\bar{p}\mathrm{He}^+$ state, the assumption of hydrogenic energy levels is unrealistic except for very high N. By using Eq. (22), one can derive the relation between the probability (density) of the capture into the (N,L) state and the probability density of the emitted electron in the form

$$\frac{dP^{J}_{L}}{dN} = \left|\frac{\partial E_{NL}}{\partial N}\right|\sum_{l}\frac{dP^{J}_{Ll}}{d\varepsilon}. \tag{24}$$

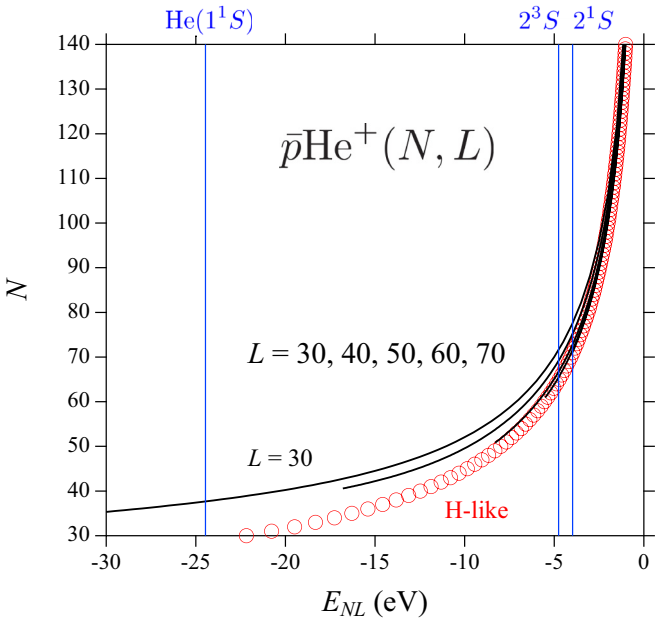

FIG. 2. (Color online) Principal quantum numbers N plotted against the bound-state energy E_{NL} of $\bar{p}\mathrm{He}^+$. Circles indicate the hydrogenic energies $-m_R/(2N^2)$. Vertical lines indicate the He energies $-I_\gamma$ ($\gamma = 1\,^1S$, $2\,^3S$, and $2\,^1S$), and the intersection points present the quantum number N satisfying the energy matching condition $-I_\gamma = E_{NL}$.

In the present study, the energy distribution of the emitted electrons is defined by

$$F(\varepsilon) = \frac{1}{\Omega_{\rm cap}} \sum_{JLl} (2J+1) \frac{dP^J_{Ll}}{d\varepsilon}, \tag{25}$$

and the state distributions of the products $\bar{p}\mathrm{He}^+$ are

$$F(N,L) = \frac{1}{\Omega_{\rm cap}} \sum_{J} (2J+1) \frac{dP^J_{L}}{dN}, \tag{26}$$

$$F(N) = \frac{1}{\Omega_{\rm cap}} \sum_{JL} (2J+1) \frac{dP^J_{L}}{dN}, \tag{27}$$

$$F(L) = \frac{1}{\Omega_{\rm cap}} \sum_{J} (2J+1) P^J_{L}. \tag{28}$$

By definition, the distribution is normalized to unity in total.

D. Breakup ionization

When the collision energy is above the ionization threshold (i.e., $E > I_\gamma$), the ionization channel ($\rightarrow \bar{p} + \mathrm{He}^+ + e$) becomes open. (Here, "ionization" is used to mean "breakup ionization".) From Eq. (22), one can distinguish between the capture and ionization channels according to the criteria $\varepsilon \gtrless E - I_\gamma$. Thus, the total capture probability becomes

$$P^J_{\rm cap} = \sum_{Ll} \int_{E-I_\gamma}^{\infty} \frac{dP^J_{Ll}}{d\varepsilon} d\varepsilon, \tag{29}$$

while the total ionization probability is given by

$$P^J_{\rm ion} = \sum_{Ll} \int_{0}^{E-I_\gamma} \frac{dP^J_{Ll}}{d\varepsilon} d\varepsilon. \tag{30}$$

The total ionization cross section $\sigma_{\rm ion}$ is

$$\sigma_{\rm ion} = \frac{\pi}{2m_R E} \sum_J (2J+1) P^J_{\rm ion}. \tag{31}$$

III. LONG-LIVED ANTIPROTONIC HELIUM

The $\bar{p}\mathrm{He}^+$ atoms produced in the capture process have the Auger decay channels

$$\bar{p}\mathrm{He}^+(N,L) \rightarrow \bar{p}\mathrm{He}^{2+}(N_+,L_+) + e, \tag{32}$$

where (N_+,L_+) are the principal and angular momentum quantum numbers of the hydrogenic $\bar{p}\mathrm{He}^{2+}$ ion. One can detect the $\bar{p}\mathrm{He}^+$ atoms in the capture process only if they have sufficiently long lifetimes. The stability against Auger decay can be discussed by using the BO potential curves [8,10–12]. Figure 3 shows the effective potentials of the $\bar{p} + \mathrm{He}^+$ and $\bar{p} + \mathrm{He}^{2+}$ systems. In this figure, the transition can take place only in the case that the (N_+,L_+) level is lower than the (N,L) level. The angular momentum change $\Delta L = |L - L_+|$ is roughly equal to the angular momentum of the Auger emitted electron. It follows that the Auger transition becomes suppressed if ΔL is large.

Since the $\bar{p} + \mathrm{He}^{2+}$ effective potentials for $L_+ \geqslant 38$ are always above the dissociation limit of $\bar{p}\mathrm{He}^+$, the $\bar{p}\mathrm{He}^{2+}$ ion has no other choice but to have $L_+ \leqslant 37$ in Eq. (32). This means that all the Auger processes of $\bar{p}\mathrm{He}^+$ with $L \gg 38$ (i.e., $\Delta L \gg 1$) should be strongly suppressed. Let us assume

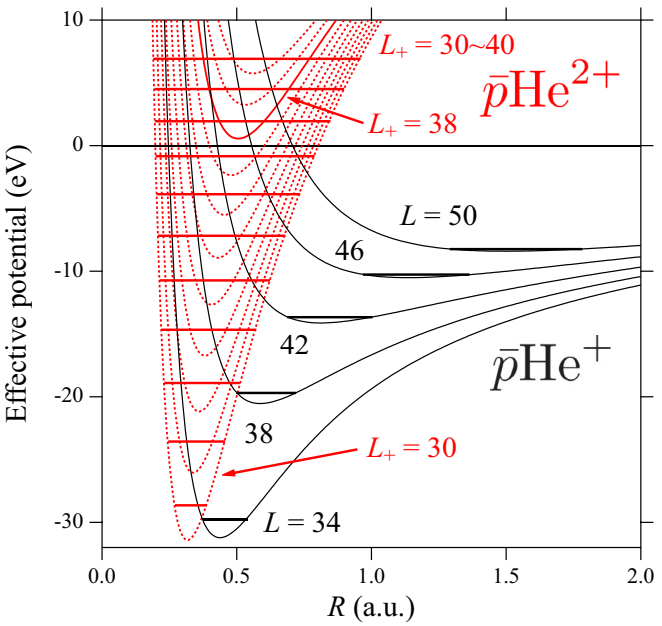

FIG. 3. (Color online) Effective potential energies of $\bar{p} + \mathrm{He}^+$ ($L = 34,38,\ldots,50$) and $\bar{p} + \mathrm{He}^{2+}$ ($L_+ = 30,31,\ldots,40$), measured from the dissociation limit ($\bar{p}\mathrm{He}^+ \rightarrow \bar{p} + \mathrm{He}^+$). Horizontal lines indicate several energy levels of $\bar{p}\mathrm{He}^+(N = L+1,L)$ (i.e., $v = 0$) and $\bar{p}\mathrm{He}^{2+}(N_+,L_+)$.

that the $\bar{p}\mathrm{He}^+$ state (N,L) is experimentally measurable within the lifetime if all the possible Auger transitions from this state have the change of $\Delta L > 2$ [3,33]. Then, one can conclude that the states with $L > 40$ would be surely observable. It should be noted that this condition holds for any value of $N > 41$, and is not limited to near-circular states $L \sim N - 1$.

In the case of $L \simeq 38$, the Auger transition with small ΔL remains energetically forbidden if the vibrational state of $\bar{p}\mathrm{He}^+$ is very low ($v \sim 0$). However, it becomes feasible for $v \gg 1$, and moreover the Franck-Condon factor of the related states becomes larger with increasing v. Thus, it is understandable that only near-circular states $L \sim N - 1$ (i.e., $v \sim 0$) are observable for $L \simeq 38$ [3,33].

In the case of $L \ll 38$, the Auger transition becomes energetically allowed also for small ΔL. Furthermore, because the equilibrium distances of $\bar{p}\mathrm{He}^+$ and $\bar{p}\mathrm{He}^{2+}$ having low angular momenta are close to each other, the Franck-Condon factor associated with the Auger transition is significant. It is hence inferred that any $\bar{p}\mathrm{He}^+$ states with $L \ll 38$ would have large Auger decay rates.

In the present calculation, the Auger channel of Eq. (32) cannot be directly taken into account. Instead, the following criterion is adopted: *The observable state of* $\bar{p}\mathrm{He}^+$ *is either any* N *if* $L > 40$ *or only* $N \sim L + 1$ *if* $L \sim 38$.

IV. GROUND-STATE HELIUM

First, let us discuss the $\bar{p}$ collisions with He atoms in the ground $1\,{}^1S$ state. The calculations were carried out at collision energies $E = 10$–40 eV, below and above the ionization threshold $I_{1\,{}^1S}$. The calculation of the electron probability density $dP^J_{Ll}/d\varepsilon$ is an essential part of the present SC method: All the important quantities are derived from $dP^J_{Ll}/d\varepsilon$ as seen in Secs. II C and II D. In Fig. 4, the electron energy distributions $F(\varepsilon)$ calculated from Eq. (25) are shown for the collision energies $E = 20$, 30, and 40 eV. It is seen that most of the electrons have energies $\varepsilon < 10$ eV. The distribution $F(\varepsilon)$ at $\varepsilon > 2$ eV does not differ very much for these collision energies E. The peak of the distribution is located at $\varepsilon \sim 1$ eV for

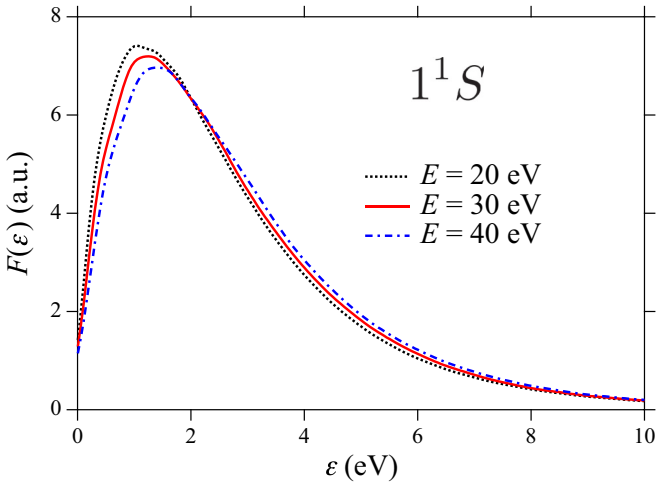

FIG. 4. (Color online) Electron energy distributions $F(\varepsilon)$ in $\bar{p}$ + He($1\,{}^1S$) at $E = 20$, 30, and 40 eV.

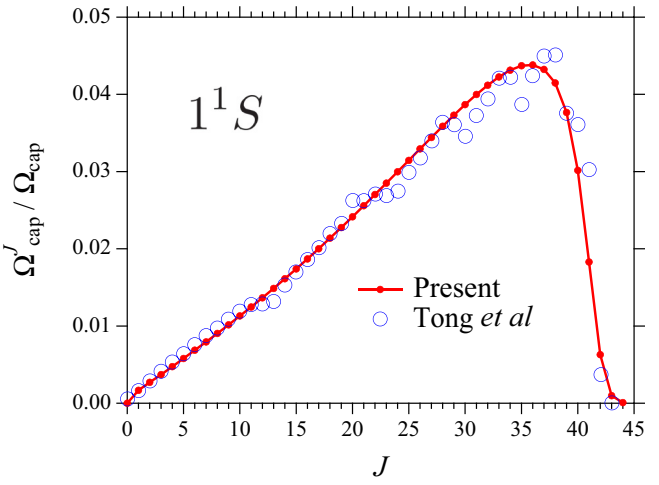

FIG. 5. (Color online) Contributions of the partial wave J to the total capture cross section, represented by $\Omega^J_{\mathrm{cap}}/\Omega_{\mathrm{cap}}$, in $\bar{p}$ + He($1\,{}^1S$) at $E = 10$ eV. The QM results of Tong *et al.* [25] are also plotted.

$E = 20$ eV, and slightly moves toward higher ε with increasing E. The same feature is found in the QM calculation of Tong *et al.* [25]. (Since they presented the convoluted distribution, a direct comparison with their results is not attempted here.)

Tong *et al.* [25] presented the J-dependent capture cross section divided by σ_{cap}, which is identical to $\Omega^J_{\mathrm{cap}}/\Omega_{\mathrm{cap}}$ in the present notation. Figure 5 compares the results of $\Omega^J_{\mathrm{cap}}/\Omega_{\mathrm{cap}}$ with the QM results of Tong *et al.* at $E = 10$ eV. Overall, the SC method reproduces the QM results except for small oscillation. The oscillation in the QM results occurs because of the nonhydrogenic level structure of $\bar{p}\mathrm{He}^+$ [25]. Since the energy conservation cannot be taken into account precisely in the SC method, the present results simply form a smooth curve. Although this is a defect in the SC theory, the overall agreement indicates that the error due to the defect is minor.

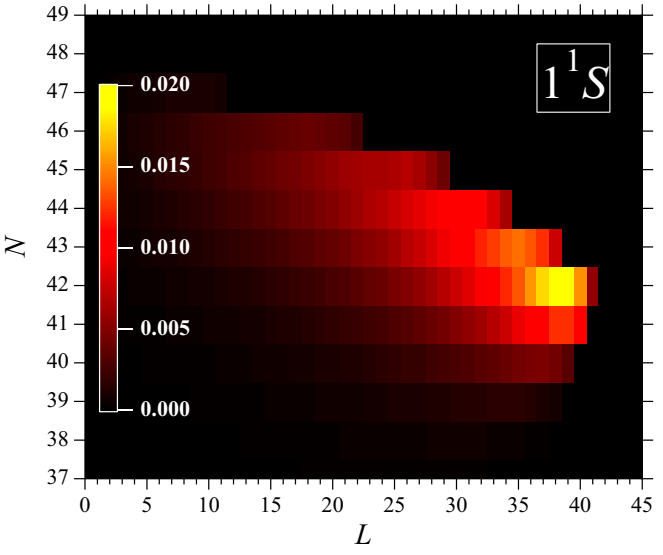

FIG. 6. (Color online) State distributions $F(N,L)$ in $\bar{p}$ + He($1\,{}^1S$) at $E = 10$ eV.

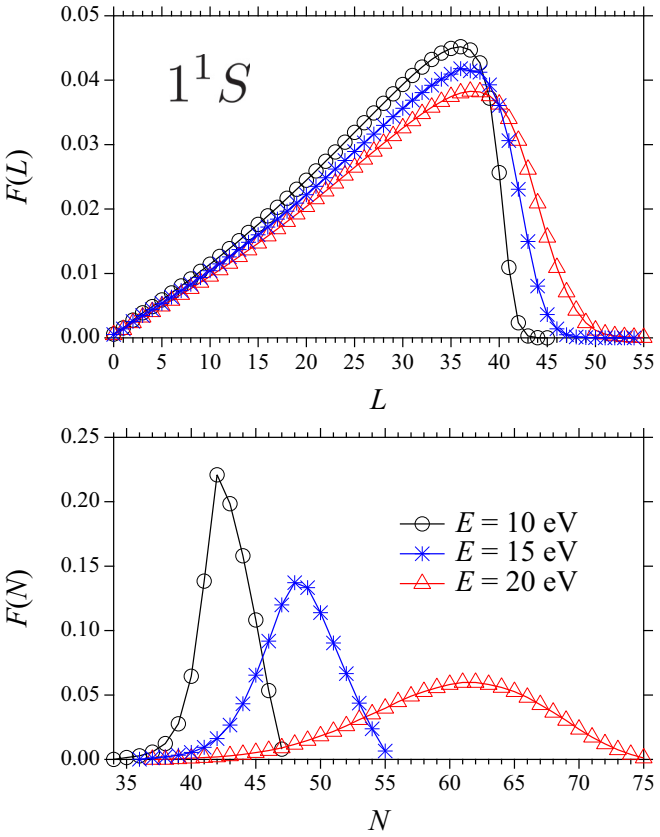

FIG. 7. (Color online) State distributions $F(L)$ and $F(N)$ in $\bar{p}$ + He($1\,^1S$) at $E = 10,\ 15$, and 20 eV.

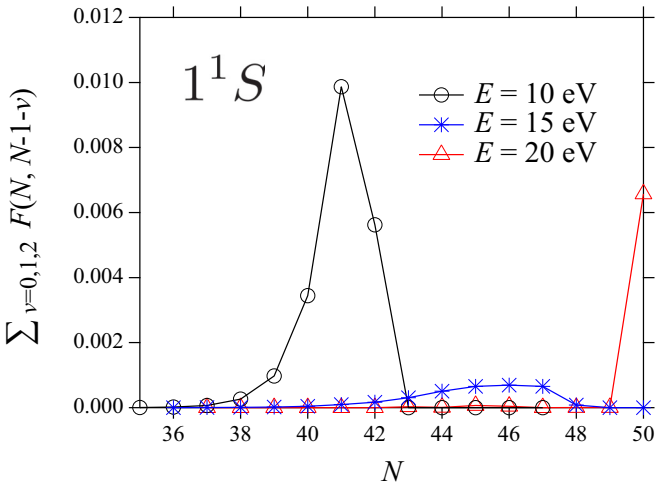

FIG. 8. (Color online) Total fractions of the capture into near-circular states $(N,N-1)+(N,N-2)+(N,N-3)$ (i.e., $v \leqslant 2$) in $\bar{p}$ + He($1\,^1S$) at $E = 10,\ 15$, and 20 eV.

Figure 6 shows the state distribution $F(N,L)$ at $E = 10$ eV, visualized as a brightness-scale image. The image features look very similar to those obtained by the QM calculation [25]. Additionally, the present and QM distributions have the maximum peak nearly at the same quantum numbers, i.e., $(N,L) = (42,39)$ and $(42,38)$, respectively. The state distributions $F(L)$ and $F(N)$ are plotted in Fig. 7 for $E = 10,\ 15$, and 20 eV. Both these distributions are shifted to higher quantum numbers as the energy E increases. Since the emitted electron can carry away only low angular momenta $l \lesssim 1$, the L-state distribution is very similar to the partial-wave (J) contribution shown in Fig. 5. By using the FMD method, Cohen [19] presented the N-state distribution of $\bar{p}\mathrm{He}^+$ at $E = 0.4$ a.u.(=10.9 eV). His result (the second peak) has the qualitatively same feature as the present one $F(N)$ at $E = 10$ eV (Fig. 7). (It should be mentioned however that the Auger effect is reflected in the FMD results.) In the CTMC calculation of Tőkési *et al.* [17], the N-state distribution for $E = 10$ eV has the maximum peak at $N = 35$, which is much lower than the present value $N = 42$ (Fig. 7). The reason for this discrepancy is probably that Tőkési *et al.* assumed the potential $V_{\bar{p}\text{-He}^+}(R)$ to have the same form as $V_{e\text{-He}^+}(R)$. This assumption would be too crude for $V_{\bar{p}\text{-He}^+}(R)$. The accuracy of the interaction $V_{\bar{p}\text{-He}^+}(R)$ is important in investigating the state distribution: For example, if a simplified form $V_{\bar{p}\text{-He}^+}(R) = -1/R$ were assumed in the present calculation, as seen from Fig. 2 and Eq. (22), the N-state distribution would be shifted to much lower N.

As discussed in section III, the information on the L-state distribution is important for evaluating the stability of $\bar{p}\mathrm{He}^+$. It is seen from Fig. 7 that the capture at $E = 10$ eV yields $L \lesssim 40$ states of $\bar{p}\mathrm{He}^+$. Therefore, when the collision energy is $E = 10$ eV, only near-circular states with $L \sim 38$ can contribute to long-lived $\bar{p}\mathrm{He}^+$. For reference, the total fraction of the capture into near-circular states (N,L) with $N - L \leqslant 3$ (or $v \leqslant 2$) is shown as a function of N for $E = 10, 15$, and 20 eV in Fig. 8. It can be seen that the capture into near-circular states with $L \sim 38$ seldom occurs at energies much higher than 10 eV. Therefore, only low-energy ($E \lesssim 10$ eV) collisions are appropriate for the production of long-lived states with $L \sim 38$. However, with increasing energy E, a notable amount of $\bar{p}\mathrm{He}^+$ atoms have $L > 40$, as seen in Fig. 7, and these are all considered to have long lifetimes regardless of whether they are in near-circular states or not. Thus, for the production of long-lived states with $L > 40$, rather high-energy ($E > 10$ eV) collisions are important.

Figure 9 compares the capture and ionization cross sections obtained by the present SC method with those of other representative (FMD [19], QM [25], and adiabatic hidden-crossing [15]) methods. Simply stated, all these results are diverse, and the agreement is not satisfactory. (See Sec. VI for further discussion.) In addition, the difference between the SC and QM results is larger than 20%. This situation is in contrast to that for the $\bar{p}$ + H system, in which the SC results always agree with the QM results within 5% errors [22,26,32], and the difference between the independent QM calculations [21,23] is insignificant. In the present study, the form of the interaction $V_{e\text{-He}^+}(R)$ is not the same as that assumed in the QM calculation. To check the effect of different $V_{e\text{-He}^+}(R)$ on the result, the SC calculation was also made by using the potential $V_{e\text{-He}^+}(R)$ of Ref. [25]. At $E = 10$ eV, the use of this potential yields $\sigma_{\mathrm{cap}} = 3.10$ a.u. while the original SC value is 3.15 a.u. Therefore, the difference in $V_{e\text{-He}^+}(R)$ is considered to be insignificant. The reason for the notable discrepancy between the QM and SC results is unknown.

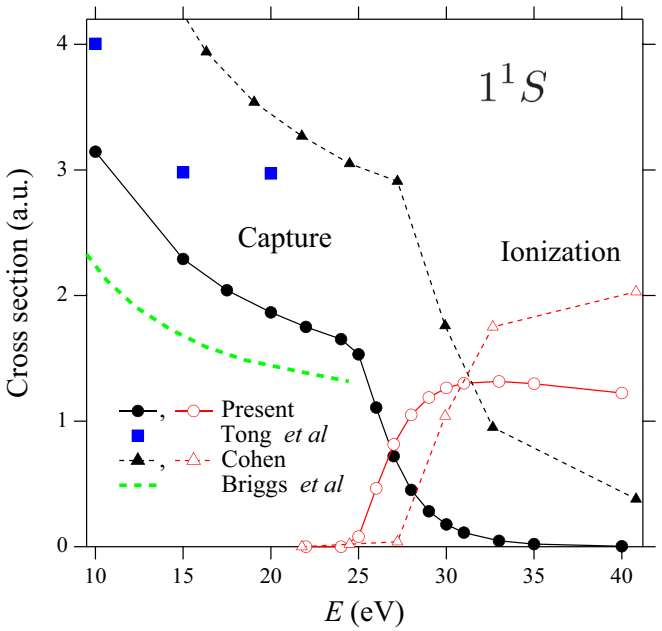

FIG. 9. (Color online) Capture (filled symbols) and ionization (open symbols) cross sections in $\bar{p} + \mathrm{He}(1\,^1S)$. The QM results of Tong *et al.* [25], the FMD results of Cohen [19], and the adiabatic hidden-crossing results of Briggs *et al.* [15] are also plotted.

Unless the energy E is so low that orbiting collisions take place, the total electron-emission cross section $\sigma_{\mathrm{tot}} = \sigma_{\mathrm{cap}} + \sigma_{\mathrm{ion}}$ may be expressed in a simple function form derived from an adiabatic ionization model [12,20], i.e.,

$$\sigma_{\mathrm{tot}}\ (\mathrm{a.u.}) = A + \frac{B}{E\ (\mathrm{eV})}, \tag{33}$$

where A and B are constants. At all the energies $E \geqslant 4$ eV, the FMD, the adiabatic hidden-crossing, and the present SC results are found to be nicely approximated by the fitting function of Eq. (33). For the present results, the fitting coefficients are $(A = 0.5852, B = 25.67)$. One can reasonably fit Eq. (33) to the QM results if the energy range is limited to $4 \leqslant E \leqslant 15$ eV. However, the fitting becomes unfavorable if the point at $E = 20$ eV is included: This data value is too large for the fitting, as can be clearly inferred from Fig. 9. Incidentally, for the $\bar{p} + \mathrm{H}$ system, the fitting coefficients are $(A = 3.726, B = 39.11)$ from the QM data [21,22].

In the present results, as the energy increases from the ionization threshold $I_{1\,^1S}$, the capture cross section drops rapidly, and the ionization cross section increases instead. It shows a transition region between the two reactive channels. In the present calculation, the width ΔE of the transition region is determined by the condition $E_{NL} = E - I_\gamma - \varepsilon < 0$ from Eq. (22), and thereby is nearly equal to the highest electron energy ε_0 at which a non-negligible amount of electrons are emitted, i.e., $\Delta E \simeq \varepsilon_0 \sim 6$ eV from Fig. 4. The FMD results also show the transition region, and the onset of the transition seems to be $E \simeq 27$ eV higher than the present value because the first ionization potential is 0.9737 a.u. in the FMD calculation [19].

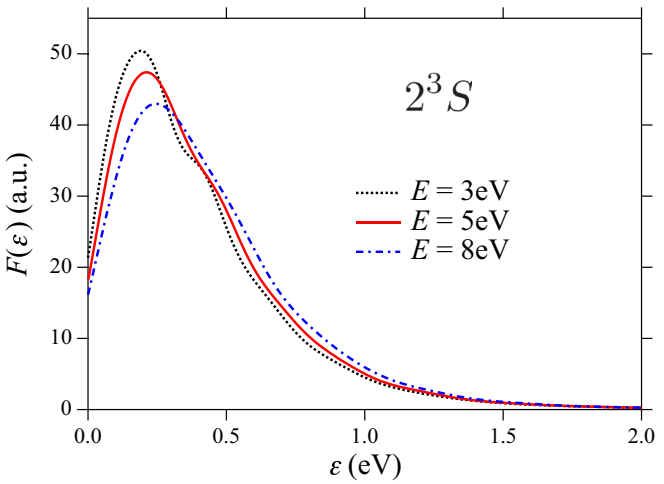

FIG. 10. (Color online) Electron energy distributions $F(\varepsilon)$ in $\bar{p} + \mathrm{He}(2\,^3S)$ at $E = 3$, 5, and 8 eV.

V. METASTABLE $2\,^3S$ AND $2\,^1S$ HELIUM

For the He target in the metastable 2^3S and 2^1S states, the calculations were carried out at collision energies $E =$ 1–8 eV. In Fig. 10, the electron energy distributions $F(\varepsilon)$ at $E = 3$, 5, and 8 eV are shown for $\mathrm{He}(2\,^3S)$. A similar result is obtained also for $\mathrm{He}(2\,^1S)$. One can see that $\varepsilon_0 \sim 1$ eV, which is much lower than $\varepsilon_0 \sim 6$ eV of the ground-state target. Figure 11 shows the state distribution $F(N,L)$ at $E = 3$ eV for $\mathrm{He}(2\,^3S)$. The image features for the metastable targets are drastically different from those for the ground-state target. The distribution in Fig. 11 has its maximum peak at the very high quantum numbers $(N,L) = (101,64)$. If the distribution $F(N,L)$ is drawn as a function of L for a fixed N, one can see that this section view shows a single peak at a middle L for $N \leqslant 103$ or for $N \geqslant 108$, double peaks for $104 \leqslant N \leqslant 107$, and a clear cut at a high L for $N \geqslant 107$. The double-peak

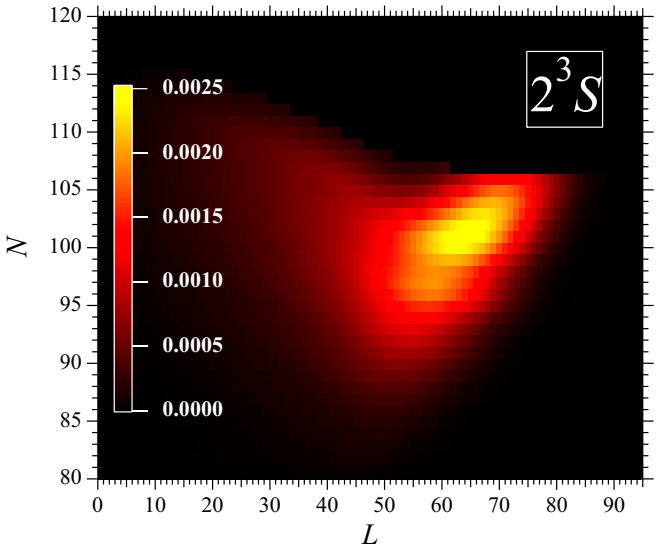

FIG. 11. (Color online) State distributions $F(N,L)$ in $\bar{p} + \mathrm{He}(2\,^3S)$ at $E = 3$ eV.

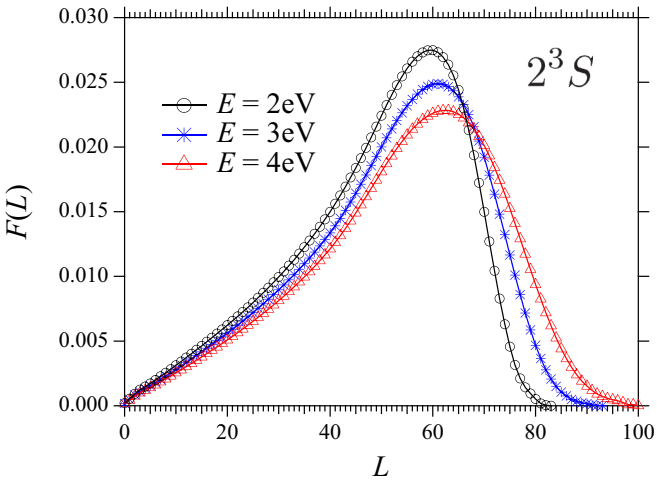

FIG. 12. (Color online) State distributions $F(L)$ in $\bar{p} + \mathrm{He}(2\,^3S)$ at $E = 2$, 3, and 4 eV.

structure is related to the fact that the $\bar{p}\mathrm{He}^+$ levels are divided into two different types: the one is hydrogenic for high L, and the other is nonhydrogenic for low L. Figure 2 shows that the same value of N corresponds to a lower-energy E_{NL} for nonhydrogenic states than for hydrogenic states. As far as the product states of $N \geqslant 107$ are concerned in the capture at $E = 10$ eV, one can see that higher-L states become energetically closed while lower-L states remain open. The border between the open and closed channels for the same N appears as the clear cut in Fig. 11. For the ground-state target, since lower-L states are predominantly produced, and the characteristic feature originating from the hydrogenic levels is missing.

Figures 12 and 13 show the L-state distributions at $E = 2$, 3, and 4 eV for the capture by $\mathrm{He}(2\,^3S)$ and $\mathrm{He}(2\,^1S)$. It seems that the behavior of the distribution function changes slightly in the vicinity of $N \sim 40$. This occurs again due to the $\bar{p}\mathrm{He}^+$ level structure. The same finding can be observed also in the $\bar{p}$ capture by Li [12]. An important distinction between

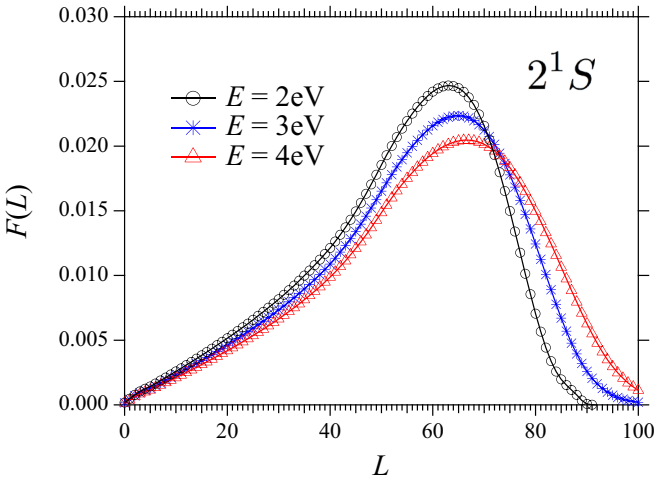

FIG. 13. (Color online) State distributions $F(L)$ in $\bar{p} + \mathrm{He}(2\,^1S)$ at $E = 2$, 3, and 4 eV.

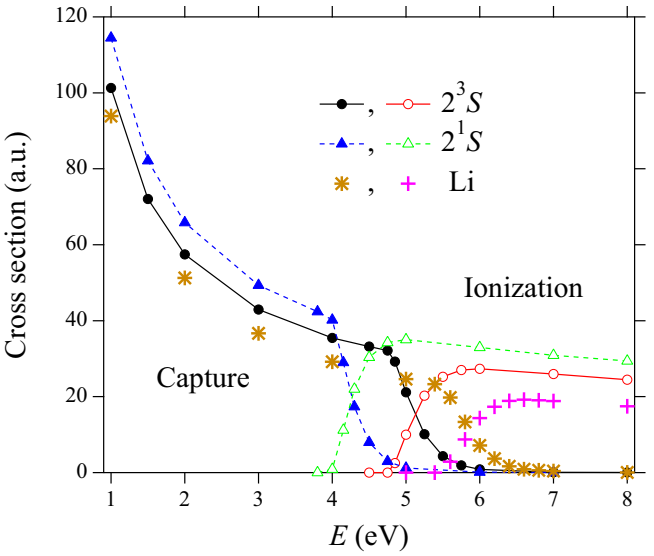

FIG. 14. (Color online) Capture and ionization cross sections in $\bar{p} + \mathrm{He}(2\,^3S)$ and $\bar{p} + \mathrm{He}(2\,^1S)$. The SC results for $\bar{p} + \mathrm{Li}$ [12] are also plotted.

the ground-state and metastable-state targets is that very high $L > 40$ states are overwhelmingly produced for the latter. As discussed in Sec. III, these high-L states are sufficiently stable against Auger decay. Therefore, it turns out that most of the $\bar{p}\mathrm{He}^+$ atoms are long lived if they are produced in $\bar{p}$ capture by He in the metastable states.

Finally, Fig. 14 shows the capture and ionization cross sections in $\bar{p} + \mathrm{He}(2\,^3S)$, $\bar{p} + \mathrm{He}(2\,^1S)$, and $\bar{p} + \mathrm{Li}$ [12]. All these reactions proceed owing to electron emission from the $2s$ subshell. For these targets, the width of the transition region just above $E = I_\gamma$ is always $\Delta E \sim 1$ eV, which comes from $\varepsilon_0 \sim 1$ eV. The total cross sections $(\sigma_{\mathrm{cap}} + \sigma_{\mathrm{ion}})$ at the same energy E are arranged in descending order, $\sigma_{\mathrm{tot}}(2\,^1S) > \sigma_{\mathrm{tot}}(2\,^3S) > \sigma_{\mathrm{tot}}(\mathrm{Li}) \gg \sigma_{\mathrm{tot}}(\mathrm{H}) > \sigma_{\mathrm{tot}}(1\,^1S)$, inversely related to the ionization potential I_γ. Here, the total cross sections $\sigma_{\mathrm{tot}}(\mathrm{H})$ for $\bar{p} + \mathrm{H}$ are taken from the QM calculations [21–23]. In the case of $2s$-electron emission also, the total cross sections are approximated by Eq. (33): The fitting coefficients are $(A = 16.77, B = 97.69)$ for $\mathrm{He}(2\,^1S)$, $(A = 13.61, B = 87.68)$ for $\mathrm{He}(2\,^3S)$, and $(A = 7.027, B = 87.30)$ for Li.

VI. SUMMARY AND DISCUSSION

The SC method has been employed to calculate the capture and ionization cross sections and the final-state distributions in low-energy collisions between $\bar{p}$ and He in the ground $(1\,^1S)$ and metastable $(2\,^3S$ and $2\,^1S)$ states. The present results of the state distributions are in good agreement with the QM results of Tong *et al.* [25]. However, the agreement for the total capture cross section is not satisfactory, in contrast to the case of the $\bar{p} + \mathrm{H}$ system. A further study is needed for the $\bar{p} + \mathrm{He}$ collisions. From the BO potential curves of $\bar{p} + \mathrm{He}^+$ and $\bar{p} + \mathrm{He}^{2+}$, the $\bar{p}\mathrm{He}^+$ atoms are found to be sufficiently stable against Auger decays if they are in near-circular states with $L \sim 38$ or in any state with $L > 40$.

For the $\bar{p}$ capture by He($1\,^1S$), near-circular states with $L \sim 38$ can be produced only in collisions at $E \lesssim 10$ eV, while the $L > 40$ states can be produced rather at $E > 10$ eV. In the experiments on $\bar{p}$ stopping by He, although collisions in a wide range of energies both below and above $E \sim 10$ eV would be involved in the capture process, very few $\bar{p}He^+$ atoms having $N > 40$ (i.e., $L > 40$) could be detected [1–3,34]. In the stopping experiments, the density of the target gas must be sufficiently high, and hence some of the primary long-lived states of $\bar{p}He^+$ produced in the capture may be destroyed by further collisions with surrounding atoms. Since such a collisional effect is more significant for higher N, the highly excited states of $N > 40$ are considered to be lost in the stopping experiments [34,35]. Recently, the MUSASHI collaboration has made progress [10,36,37], and those researchers intend to experimentally investigate $\bar{p}$ collisions with atoms and molecules using the crossed-beam technique under ultrahigh-vacuum conditions. In such experiments, one can expect that the existence of long-lived $\bar{p}He^+$ with high $L > 40$ might be confirmed. If the He target is excited in metastable ($2S$) states, most of the products $\bar{p}He^+$ have $L > 40$. Hence, the use of metastable He targets would significantly raise the production efficiency of long-lived $\bar{p}$He.

As in the QM study of Tong *et al.* [25], the present calculation was carried out by assuming that one electron is passive and distinguishable from the other, active electron. This assumption may be controversial especially in treating a ground-state He target, in which the two electrons occupy the same $1s$ subshell. If the spatial part of the singlet two-electron wave function can be written in a simple product form, the probabilities of single-electron emission ($P^J_{\rm single}$) and of direct double-electron emission ($P^J_{\rm double}$) may rather have to be expressed as [38,39]

$$P^J_{\rm single} = 2P^J_1\left(1 - P^J_1\right), \quad P^J_{\rm double} = \left(P^J_1\right)^2, \qquad (34)$$

where P^J_1 is the electron emission probability obtained from the one-electron problem (independent-electron model). The latter form $P^J_{\rm double}$ has been used for estimating the double-ionization probability of He by laser irradiation and by high-energy ion impact [38–40]. In the present case, if the probability P^J_1 is assumed to be given by $P^J_{\rm cap} + P^J_{\rm ion}$, then one has $P^J_{\rm single} \sim 0.48$ and $P^J_{\rm double} \sim 0.36$ ($P^J_1 \sim 0.6$ at $E = 10$ eV and probably also at $E \ll 10$ eV). This may suggest that significant direct double-electron emission occurs even at very low energies. However, the FMD study [19] shows that this is not the case. At the present time, the role of direct double-electron emission and its significance in the capture process remain obscure. Since it has become possible to properly treat the two electrons in a SC study of $\bar{p} + $ He ionization at high energies (>1 keV) [39], a similar approach will be developed also for the $\bar{p}$ capture by He in the not-too-distant future.

In the one-active-electron model, the single-ionization cross section of $\bar{p} + $ He($1\,^1S$) at high energies (>1 keV) has usually been given by the one-active-electron ionization cross section multiplied by a factor of 2 [39]. The reason for this is that one cannot know which of the two electrons is active or passive. In previous studies on $\bar{p}$ capture by He($1\,^1S$) that were based on the one-electron approximation, the multiplying fact of 2 was missing. In the present study also, for the purpose of comparing directly with the cross sections of the QM [25] and other one-electron-approximation methods, the multiplying factor has not been applied to the present results shown in Fig. 9. [The multiplying factor has no effect on the state distributions $F(N,L)$.] If the capture and ionization cross sections are compared with experiments, the present results should be multiplied by 2. Incidentally, the present results for $2\sigma_{\rm tot}$ become close to the total emission cross sections (not multiplied by 2) obtained by the FMD method [19], which classically treats the two electrons on an equal footing. Attention should be paid to the capture cross sections of $\bar{p} + $ He($1\,^1S$) if they were calculated by the one-electron approximation.

The single-ionization cross section of $\bar{p} + $ He($1\,^1S$) decreases with decreasing E in the 1–50 keV region [39], while the present total emission cross section $\sigma_{\rm tot}$ (or $2\sigma_{\rm tot}$) decreases with increasing E in the region below 50 eV. If both these results are correct, the ionization cross section will have a minimum at an intermediate energy between 50 eV and 1 keV. For the ionization of H by $\bar{p}$ impact, several theoretical studies show that the cross section is rather flat in the intermediate energy region [39]. This is considered to be due to the attractive force working between $\bar{p}$ and H, i.e., there is a gross deviation from straight-line trajectories. It is to be understood that the same effect becomes important at intermediate energies also for the $\bar{p} + $ He collisions. Further study of the ionization of He by $\bar{p}$ impacts in the intermediate-energy region would be very interesting.

[1] M. Iwasaki, S. N. Nakamura, K. Shigaki, Y. Shimizu, H. Tamura, T. Ishikawa, R. S. Hayano, E. Takada, E. Widmann, H. Outa, M. Aoki, P. Kitching, and T. Yamazaki, Phys. Rev. Lett. **67**, 1246 (1991).

[2] T. Yamazaki, E. Widmann, R. S. Hayano, M. Iwasaki, S. N. Nakamura, K. Shigaki, F. J. Hartmann, H. Daniel, T. von Egidy, P. Hofmann, Y. S. Kim, and J. Eades, Nature (London) **361**, 238 (1993).

[3] T. Yamazaki, N. Morita, R. S. Hayano, E. Widmann, and J. Eades, Phys. Rep. **366**, 183 (2002).

[4] M. Hori, Phys. Rep. **403-404**, 337 (2004).

[5] R. S. Hayano, M. Hori, D. Horváth, and E. Widmann, Rep. Prog. Phys. **70**, 1995 (2007).

[6] G. T. Condo, Phys. Lett. **9**, 65 (1964).

[7] J. E. Russell, Phys. Rev. Lett. **23**, 63 (1969).

[8] R. Ahlrichs, O. Dumbrajs, H. Pilkuhn, and H. G. Schlaile, Z. Phys. A **306**, 297 (1982).

[9] O. I. Tolstikhin, S. Watanabe, and M. Matsuzawa, Phys. Rev. A **54**, R3705(R) (1996).

[10] Y. Yamazaki, Nucl. Instrum. Methods Phys. Res., Sect. B **154**, 174 (1999).

[11] I. Shimamura, M. Kimura, and Y. Korenman, in *Abstracts of Contributed Papers*, edited by Y. Itikawa, K. Okuno, H. Tanaka,

A. Yagishita, and M. Matsuzawa (Local Organizing Committee of XXI ICPEAC, Sendai, Japan, 1999), p. 446.
[12] K. Sakimoto, Phys. Rev. A **84**, 032501 (2011).
[13] J. S. Cohen, R. L. Martin, and W. R. Wadt, Phys. Rev. A **27**, 1821 (1983).
[14] G. Ya. Korenman, Hyperfine Interact. **101-102**, 81 (1996).
[15] J. S. Briggs, P. T. Greenland, and E. A. Solov'ev, J. Phys. B **32**, 197 (1999).
[16] J. Révai and N. Shevchenko, Eur. Phys. J. D **37**, 83 (2006).
[17] K. Tőkési, B. Juhász, and J. Burgdörfer, J. Phys. B **38**, S401 (2005).
[18] W. A. Beck, L. Wilets, and M. A. Alberg, Phys. Rev. A **48**, 2779 (1993).
[19] J. S. Cohen, Phys. Rev. A **62**, 022512 (2000).
[20] J. S. Cohen, Rep. Prog. Phys. **67**, 1769 (2004).
[21] K. Sakimoto, Phys. Rev. A **65**, 012706 (2001).
[22] K. Sakimoto, Phys. Rev. A **70**, 064501 (2004).
[23] X. M. Tong, K. Hino, and N. Toshima, Phys. Rev. Lett. **97**, 243202 (2006).
[24] K. Sakimoto, Phys. Rev. A **88**, 012507 (2013).
[25] X. M. Tong, K. Hino, and N. Toshima, Phys. Rev. Lett. **101**, 163201 (2008).
[26] K. Sakimoto, Phys. Rev. A **66**, 032506 (2002).
[27] D. Rabli, M. Gargaud, and R. McCarroll, Phys. Rev. A **64**, 022707 (2001).
[28] C. E. Moore, *Atomic Energy Levels*, Natl. Bur. Stand. (US) Circ. No. 467 (US GPO, Washington, DC, 1949).
[29] I. Shimamura, Phys. Rev. A **46**, 3776 (1992).
[30] M. Rérat, M. Caffarel, and C. Pouchan, Phys. Rev. A **48**, 161 (1993).
[31] M. Masili and A. F. Starace, Phys. Rev. A **68**, 012508 (2003).
[32] S. Yu. Ovchinnikov and J. H. Macek, Phys. Rev. A **71**, 052717 (2005).
[33] V. I. Korobov and I. Shimamura, Phys. Rev. A **56**, 4587 (1997).
[34] M. Hori, J. Eades, R. S. Hayano, T. Ishikawa, J. Sakaguchi, T. Tasaki, E. Widmann, H. Yamaguchi, H. A. Torii, B. Juhász, D. Horváth, and T. Yamazaki, Phys. Rev. Lett. **89**, 093401 (2002).
[35] M. Hori, J. Eades, E. Widmann, and T. Yamazaki, R. S. Hayano, T. Ishikawa, H. A. Torii, T. von Egidy, F. J. Hartmann, B. Ketzer, C. Maierl, R. Pohl, M. Kumakura, N. Morita, D. Horváth, and I. Sugai, Phys. Rev. A **70**, 012504 (2004).
[36] H. A. Torii, Y. Nagata, H. Imao, V. L. Varentsov, N. Kuroda, M. Shibata, K. Ogata, H. Toyoda, T. Shimoyama, Y. Enomoto, H. Higaki, Y. Kanai, A. Mohri, and Y. Yamazaki, in *Proceedings of the Workshop on Cold Antimatter Plasmas and Application to Fundamental Physics*, edited by Y. Kanai and Y. Yamazaki, AIP Conf. Proc. No. 1037 (AIP, New York, 2008), p. 297.
[37] N. Kuroda, H. A. Torii, Y. Nagata, M. Shibata, Y. Enomoto, H. Imao, Y. Kanai, M. Hori, H. Saitoh, H. Higaki, A. Mohri, K. Fujii, C. H. Kim, Y. Matsuda, K. Michishio, Y. Nagashima, M. Ohtsuka, K. Tanaka, and Y. Yamazaki, Phys. Rev. Spec. Top.–Accel. Beams **15**, 024702 (2012).
[38] D. G. Lappas and R. van Leeuwen, J. Phys. B **31**, L249 (1998).
[39] T. Kirchner and H. Knudsen, J. Phys. B **44**, 122001 (2011).
[40] L. A. Wehrman, A. L. Ford, and J. F. Reading, J. Phys. B **29**, 5831 (1996).